Editors' Suggestion | Featured in Physics

Magnetic Solitons in a Spin-1 Bose-Einstein Condensate

X. Chai,[1,†] D. Lao,[1,†] Kazuya Fujimoto,[2,3] Ryusuke Hamazaki,[4,5] Masahito Ueda,[4,6,7] and C. Raman[1,*]

[1]School of Physics, Georgia Institute of Technology, 837 State Street, Atlanta, Georgia 30332, USA
[2]Institute for Advanced Research, Nagoya University, Nagoya 464-8601, Japan
[3]Department of Applied Physics, Nagoya University, Nagoya 464-8603, Japan
[4]Department of Physics, University of Tokyo, 7-3-1 Hongo, Bunkyo-ku, Tokyo 113-0033, Japan
[5]Nonequilibrium Quantum Statistical Mechanics RIKEN Hakubi Research Team, RIKEN Cluster for Pioneering Research (CPR), RIKEN iTHEMS, Wako, Saitama 351-0198, Japan
[6]Institute for Physics of Intelligence, University of Tokyo, 7-3-1 Hongo, Bunkyo-ku, Tokyo 113-0033, Japan
[7]RIKEN Center for Emergent Matter Science (CEMS), Wako, Saitama 351-0198, Japan

(Received 2 January 2020; accepted 26 May 2020; published 15 July 2020)

Vector solitons are a type of solitary or nonspreading wave packet occurring in a nonlinear medium composed of multiple components. As such, a variety of synthetic systems can be constructed to explore their properties, from nonlinear optics to ultracold atoms, and even in metamaterials. Bose–Einstein condensates have a rich panoply of internal hyperfine levels, or spin components, which make them a unique platform for exploring these solitary waves. However, existing experimental work has focused largely on binary systems confined to the Manakov limit of the nonlinear equations governing the soliton behavior, where quantum magnetism plays no role. Here we observe, using a "magnetic shadowing" technique, a new type of soliton in a spinor Bose–Einstein condensate, one that exists only when the underlying interactions are antiferromagnetic and which is deeply embedded within a full spin-1 quantum system. Our approach opens up a vista for future studies of "solitonic matter" whereby multiple solitons interact with one another at deterministic locations.

DOI: 10.1103/PhysRevLett.125.030402

Ultracold atoms have opened a new arena for the exploration of nonlinear behavior with unique experimental tools available. A prime example of this has been the fruitful study of soliton nonlinearities [1–9]. Solitons are ubiquitous in the natural world, from the realm of shallow water waves [10] to biological systems [11] and even extending into early universe cosmology [12]. Vector solitons—those containing more than one wave component—have been observed in metamaterials [13] and have practical applications for optical communication [14,15]. In quantum systems such as photons or Bose–Einstein condensates (BECs), such vector nonlinearities offer a window into complex many-body dynamics and offer possibilities for quantum communication and information processing [16]. The multiple flavors available in Bose gases due to the rich variety of internal hyperfine spin components have enabled a number of theoretical and experimental works on vector solitons [17–23]. Until now, however, such works have largely explored the Manakov limit of the nonlinear equations. Little seems to be known about the physics outside of this regime, i.e., the connection between binary solitons and higher spin objects, including $F = 1$ spinors, where the underlying magnetic interactions between species play an important role [24]. Very recent theoretical work has explored polarization waves outside of the Manakov limit [25] and found an exact solution under the assumption of a uniform total density [26]. It has also explored the connection between solitons and thermalization of nonequilibrium Bose gases [27], where spin-spin interactions play an important role. However, only one such experiment has been reported [28], and a comprehensive description of nonlinear phenomena including these magnetic interactions has yet to emerge.

This work takes an important step forward by providing the first experimental evidence of the magnetic soliton predicted by [26] in a quasi-one-dimensional sodium spinor Bose–Einstein condensate. We use magnetic phase imprinting to experimentally create solitons in an equal mixture of the two hyperfine components $F = 1, m \equiv m_F = \pm 1$. To our knowledge, this method has only been explored numerically [29]. For spin-1 BECs with antiferromagnetic interactions, the spin-dependent interaction coefficient $g_s > 0$ [24]. This in turn implies a positive difference $\delta g = 2g_s > 0$ between intra- and interspecies interaction strengths for these two hyperfine levels [30], a prerequisite for the magnetic soliton solution of [26]. Thus, we have created vector solitons in a non-Manakov system. A powerful tool at our disposal is the availability of local *in situ* spin measurements that access the full three-component hyperfine manifold in order to probe the phase profile of the solitons in a manner not typically possible with binary mixtures.

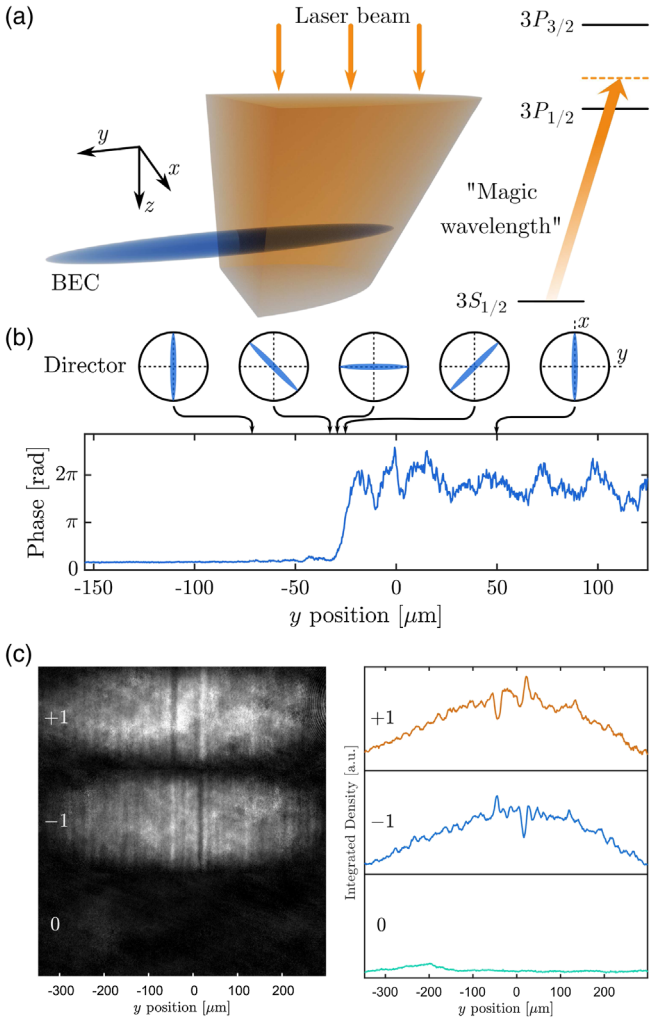

FIG. 1. Using a magnetic shadow to create magnetic solitons. (a) A sodium BEC prepared in an equal superposition of $m = \pm 1$ hyperfine states is illuminated by a pulse of far-off resonance, circularly polarized light that creates an effective magnetic field due to vector light shifts. The use of a magic wavelength eliminates scalar shifts of the $3S_{1/2}$ level due to destructive interference between contributions from the $3P_{1/2}$ and $3P_{3/2}$ levels. A knife edge placed in the beam is imaged onto the atom cloud, resulting in a "magnetic" shadow whose edge width (10% to 90%) is 8 μm. (b) Across the 8 μm transition region, the effective magnetic field gradient causes differential Larmor precession that, after 120 μs, results in a 2π phase winding and a magnetic instability. Shown schematically is the gradient-induced twisting of the nematic director for these two spin states. (c) Magnetic soliton formation at $t = 20$ ms after application of the pulse. Due to the global conservation of spin, a positive and negative pair of magnetic solitons are created. Positively magnetized solitons are seen as a density hump (dip) in the $+1(-1)$ clouds on the right side of the cloud and a corresponding negatively magnetized soliton on the left side of the cloud. Images were taken after 9 ms time of flight with Stern–Gerlach separation, with corresponding one-dimensional density profiles obtained from the data as described in [30].

Bose–Einstein condensates were prepared in the above spin mixture, with details given in the Supplemental Material [30]. Crucially, in our experiment the negative quadratic Zeeman shift strongly suppresses the $m = 0$ component to $< 5\%$ fraction of the total atom number, resulting in a binary system. Although the ground state order parameter is principally nematic, i.e., without any global magnetization, nonetheless there can be magnetic excitations in which the density difference $n_1 - n_{-1}$ is locally nonzero. One such excitation is a magnetic soliton. As predicted by Qu *et al.* [26], it consists of a density hump of one species atop a density dip in the other, so that in one dimension y, the density profile of each species is given by

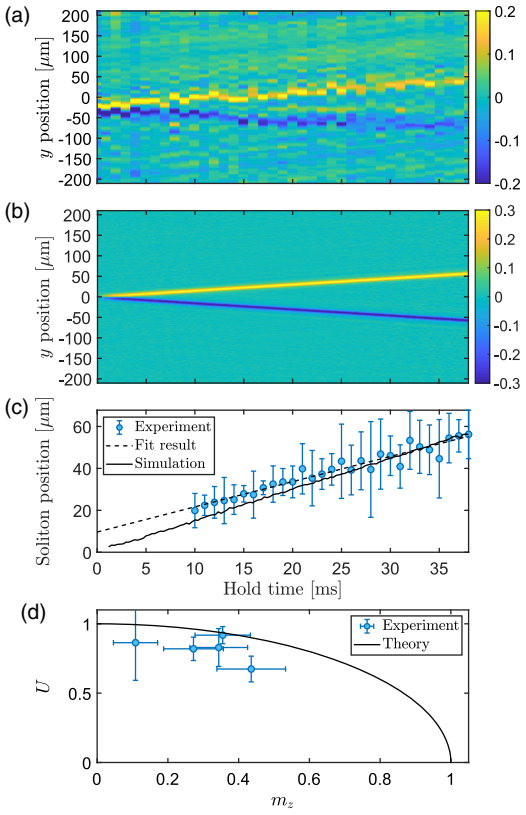

FIG. 2. Magnetic soliton formation and propagation. (a) Space-time plot of magnetization profiles $m_z(y,t)$ for different hold times after phase imprinting. Two slowly moving, unipolar magnetic structures (the magnetic solitons) with velocity $v_S = \pm 1.20$ mm/s, beginning to separate by ≈ 9 ms, were observed. (b) Numerical simulation by solving the one-dimensional Gross–Pitaevskii equation for the same parameters used in the experiment. (c) Soliton position versus time for both experiment (circles) and theory (solid black line). Dashed line is a straight line fit to the experimental data. (d) Comparison of soliton velocity $U = V/c_s$ and peak magnetization m_z. Data were obtained by varying the imprinted phase, as discussed in the text. Experimental error bars are $\pm 2\sigma$ uncertainty in the measured velocity. Solid line shows the universal curve $U = \sqrt{1 - m_z^2}$.

$$n_{1,2} = \frac{n_0}{2}\left[1 \pm \sqrt{1-U^2}\,\mathrm{sech}\left(\sqrt{1-U^2}(y-Vt)/\xi_{sp}\right)\right], \quad (1)$$

where n_0 is a uniform background total density, $U = V/c_s$ the soliton velocity normalized to that of spin waves, and $c_s = \sqrt{n_0 \delta g/(2m)}$ (see Supplemental Material [30]). The width of the soliton depends upon the spin healing length $\xi_{sp} = \hbar/\sqrt{2mn_0\delta g}$. For our cigar-shaped BEC with aspect ratio ≈70, we average the density profile over the two transverse dimensions to obtain $\bar{c}_s = c_s/\sqrt{2} = 1.47 \pm 0.17$ mm/s and $\bar{\xi}_{sp} = \sqrt{2}\xi_{sp} = 0.92 \pm 0.10$ μm, respectively, using standard time-of-flight expansion and the value of $\delta g/g = 0.07$ given in Ref. [35]. Hereafter, c_s and ξ_{sp} refer exclusively to the radially averaged parameters without notating the bar. In addition, the relative phase between the two species undergoes a π-phase jump across the soliton [26]. The analytical solution of Eq. (1) is dynamically stable only for $\delta g > 0$, confirmed also by numerical simulations in one dimension of the three-component Gross–Pitaevskii equation (see the details in Supplemental Material [30]).

We utilized a magnetic "shadowing" technique to create the solitons, as illustrated in Fig. 1(a). The vector light shift of a circularly polarized, "magic wavelength" laser beam [36] changed only the relative phase between $m = \pm 1$ in the vicinity of a knife edge without affecting the overall density. Thus, no dark solitons were created as in [1,2,18,20]. The magnetic shadow induces differential Larmor precession rates across this region [see Fig. 1(b)]. A 120 μs light pulse duration resulted in a 2π relative phase step (see Supplemental Material [30]). The opposite momentum imparted to $m = \pm 1$ atoms resulted in an instability that decays into a pair of magnetic solitons with opposite value of m_z. The global conservation of magnetization therefore plays an important role in the dynamics of phase engineering—without processes that change $n_1 - n_2$, the solitons must be produced in pairs of equal and opposite magnetization.

Figure 1(c) shows time-of-flight Stern–Gerlach images of the three spin states taken 20 ms after the phase imprinting pulse and corresponding one-dimensional density distributions obtained from the data [30]. Equal and opposite density regions appear in the $m = \pm 1$ states corresponding to the two magnetic solitons that were created. Similar work on dark-bright solitons has used the counterflow instability [21]. Our approach, by contrast, is deterministic, since solitons were placed at the knife edge location at an exact instant of time, opening new possibilities for soliton engineering. We note that magic wavelength methods have been used to excite small amplitude magnons in ferromagnetic spinor BECs via phase imprinting [37] and to selectively create spin waves without phase imprinting [38].

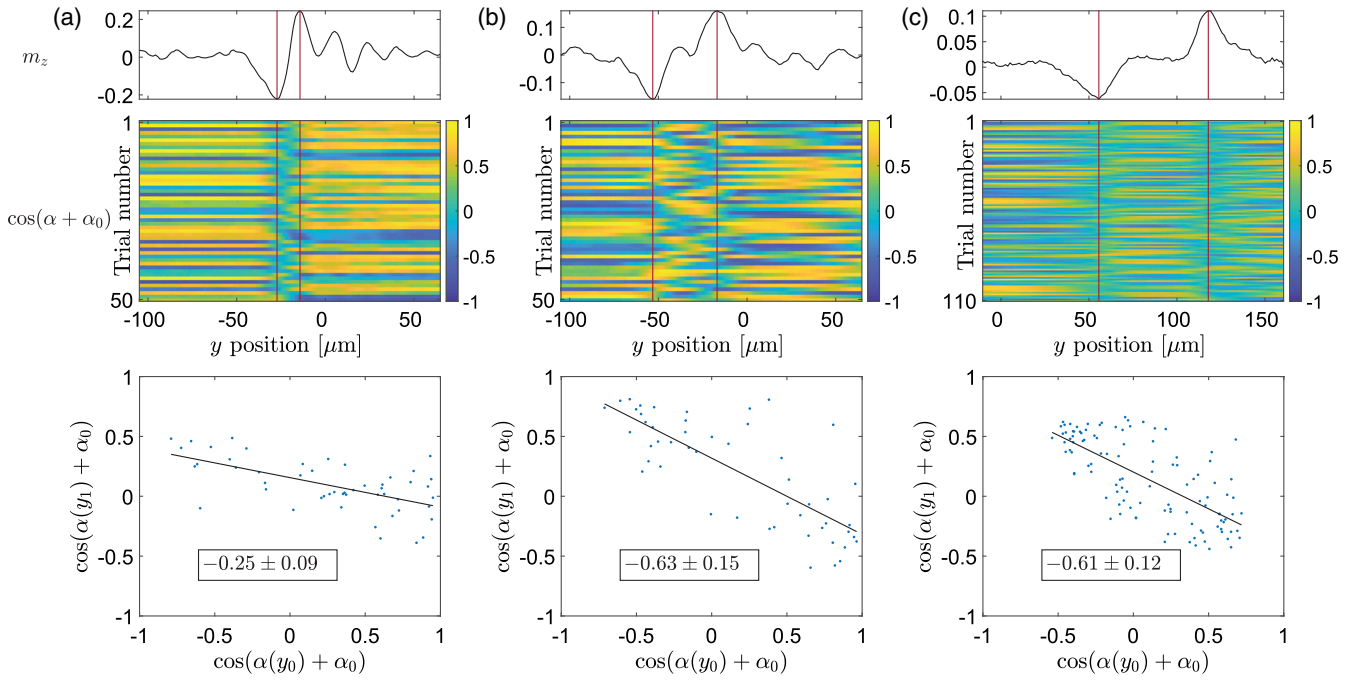

FIG. 3. The phase jump of the soliton. (a), (b), and (c) Images (second row) show spatially resolved Ramsey spectroscopy measurements of $\cos(\alpha(y) + \alpha_0)$, where $\alpha(y)$ is the phase difference between the two spin components and α_0 is the background phase difference due to magnetic field fluctuation or field inhomogeneity for (50, 50, and 110) independent runs and hold times of (0, 10, and 20) ms, respectively. Plots (upper row) show the position of the magnetic soliton pairs appearing in the corresponding magnetization data. Plots (lower row) show the negative correlation coefficients for $\cos\alpha$ between points y_0 and y_1 to the left and right, respectively, of the leftmost soliton, showing that the solitons are a domain wall across which the nematicity changes sign. Each data point represents a single trial. Here $y_0 = (-67.34, -67.34, 27.20)$ μm and $y_1 = (-20.72, -34.97, 86.77)$ μm, for (a), (b), and (c), respectively.

Figure 2(a) shows our principal data, where we have measured both the magnetization and phase profiles of the magnetic solitons. In panel 2(a) we have plotted the time evolution of the one-dimensional magnetization $m_z(y,t)$ in the form of a spacetime diagram. These data were normalized as $m_z(y,t) = 1/2(n_1/n_1^0 - n_2/n_2^0)$ to the density profiles n_i^0 without phase imprinting to remove background density variations, including the Thomas–Fermi density profile of the cloud, as detailed in the Supplemental Material [30]. It also rendered our data less sensitive to small differences from an equal spin mixture and to background magnetic field gradients. The phase step becomes rapidly converted into a positive and negative magnetization domain. Due to the very narrow transition region of 8 μm, these domains have already formed within the finite duration phase imprinting pulse. Once the pulse is over, these two domains, whose size is of the order of the width of the knife edge region, begin to separate from one another. They propagate outward as a pair of solitons whose velocity $|V| = 1.20 \pm 0.12$ mm/s, which is $\approx 0.82 c_s$ for our system. Thus, the solitons are seen to travel slower than the speed of spin sound. According to the theoretical prediction of [26] and Eq. (1) for a homogeneous binary system, the peak value of the magnetization pulse is related to the soliton velocity by a simple formula $|m_z| = \sqrt{1 - U^2}$. For our system the prediction is $|m_z| \approx 0.26$ and is consistent with our measured data. Numerical simulations in one dimension are also in very good agreement.

We also varied the pulse duration, and therefore the imprinted phase of the soliton, for five values: 70,120,170, and 220 μs at 0.5 mW laser power and 80 μs at 0.8 mW laser power. As the imprinted phase increased, we observed the soliton magnetization to increase, while its velocity became slower. The measured soliton velocity and magnetization shown in Fig. 2(d) show evidence of a weak inverse correlation in spite of relatively large error bars, according to the theoretical prediction $|m_z| = \sqrt{1 - U^2}$ [26]. The discrepancy between theory and experiment in Fig. 2(d) is likely due to the fact that time-of-flight absorption imaging reduced the measured magnetization contrast.

Our system is a two-component spinor embedded in an overall three-component gas. This allows us to employ atomic magnetometry to observe the soliton phase jump directly *in situ* in contrast to prior work using outcoupling via Bragg scattering [2]. To this end, we used spatially resolved Ramsey spectroscopy, as shown in Fig. 3, to quantify the relative phase $\alpha = \alpha(y)$ between spin states $m = \pm 1$ using a second, fast radio frequency $\pi/2$ pulse of 160 μs. $\cos\alpha(y)$ was determined from the three spin populations and the measured magnetization [30].

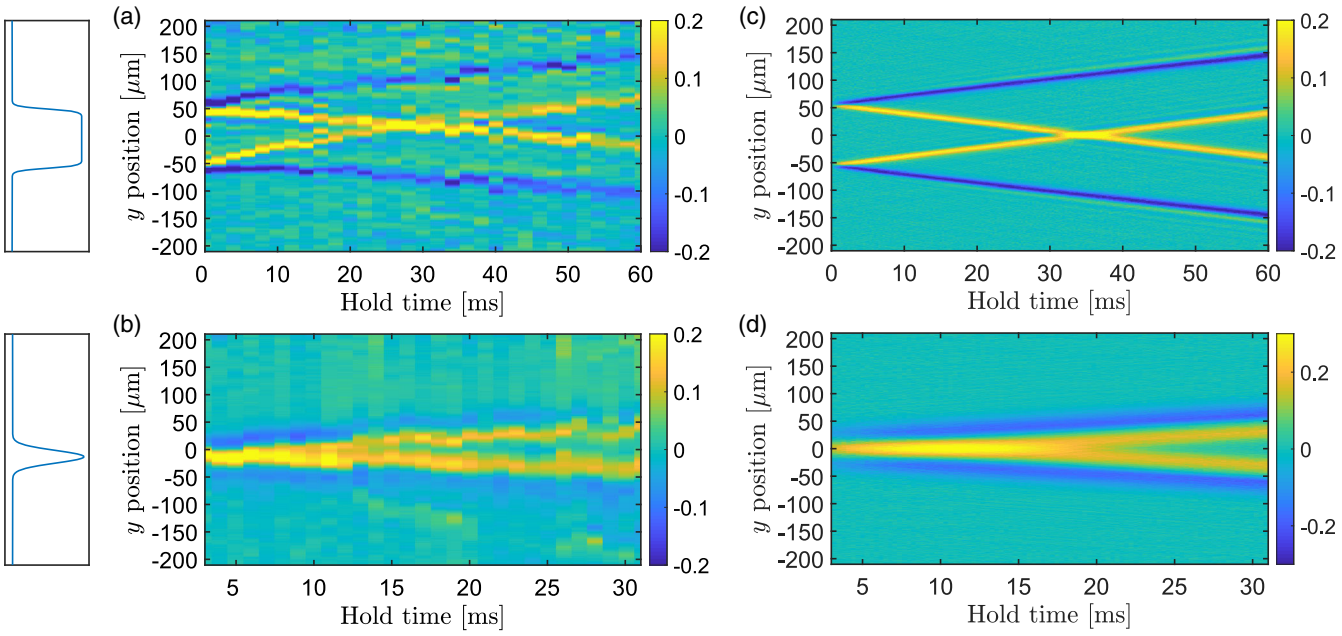

FIG. 4. Engineering multiple soliton collisions at different points in time. (a) Two knife edges created a flattop beam with 110 μm width and 8 μm edges on both sides. Two soliton pairs are created with mirror symmetric magnetization patterns. Two positively magnetized solitons (yellow lines in the spacetime plot) passed through one another 25 ms after imprinting. (b) A tightly focused phase imprinting beam with 20 μm Gaussian waist created two soliton pairs starting from nearly the same location, so that the collision of the inner two positive solitons happens nearly immediately. (c) and (d) are the corresponding numerical simulations of the one-dimensional Gross–Pitaevskii equation for the experimental parameters in (a) and (b), respectively. The phase profiles shown to the left of the data are fits to the measured laser beam profiles using (upper) a pair of spatially separated hyperbolic tangent functions and (lower) a Gaussian beam.

Figure 3 shows the result of this experiment for hold times of 0, 10, and 20 ms in panels (a), (b), and (c), respectively. The second-row panel contains, respectively, 50, 50, and 110 separate realizations of the experiment. These were taken to average out bias magnetic field fluctuations that lead to variations in the absolute phase difference α_0 between the two magnetically sensitive states. In spite of these fluctuations, there is a clear discontinuity in the measured value of $\cos\alpha$ at the location of each soliton. The spacing between solitons was 13, 36, and 62 μm for $T = 0$, 10, and 20 ms, respectively, as determined separately by magnetization measurements of the type shown in Fig. 2 and plotted in the upper panels of Fig. 3. The lower panels demonstrate the negative correlation between measurements of $\cos\alpha(y)$ for two points y_0 and y_1 on opposite sides of the leftmost soliton (values for y_0 and y_1 are given in the figure caption). The measured negative slopes were greater than -1 due to residual magnetic field fluctuations and the finite contrast of the measurement of $S(y)$. This negative correlation is consistent with a division of the nematicity N_{xx} into two regions, as expected for magnetic soliton solutions [26,27].

A key advantage of the magnetic shadow technique is the ability to coherently engineer multiple solitons and to observe their interactions. While dark solitons generally pass through one another undisturbed [39], magnetic soliton behavior is not as well studied, and both positive-positive and negative-positive collisions can occur. The latter have been predicted to form bound states that can result in annihilation of the pair [27].

We demonstrated this capability using two experiments shown in Figs. 4(a) and 4(b) with the corresponding numerical simulations in Figs. 4(c) and 4(d). In Fig. 4(a), we used two knife edges to create a flattop beam that generated four solitons, the inner two encountering each other at a time of 25 ms and passing through undisturbed. In Fig. 4(b), a tightly focused laser beam created two soliton pairs starting from nearly the same location, so that the collision happens nearly immediately. The resulting magnetization for longer times resembled two pairs of copropagating magnetic solitons with opposite magnetization. In all cases, the one-dimensional simulations showed very good agreement with the measured results.

Magnetic solitons in a highly elongated spin-1 BEC were created by the method of magnetic phase imprinting, and good agreement was observed with numerical simulations based on the one-dimensional Gross–Pitaevskii equation. Unlike turbulent methods of creating solitons, our technique of "magnetic shadowing" allows for coherent spin structures to be created and followed dynamically with very high purity (no spurious phonon creation, for example). The creation of oppositely magnetized soliton pair collisions will enable the study of universal relaxation dynamics of spin-1 Bose–Einstein condensates [27].

We acknowledge useful conversations with Carlos Sademelo and Colin Parker. This work acknowledges NSF Grant No. 1707654 and KAKENHI Grant Nos. JP18H01145, JP19K14628, JP19H01824, and JP15H05855 from the Japan Society for the Promotion of Science. R. H. was supported by a JSPS fellowship (JSPS KAKENHI Grant No. JP17J03189).

Note added in proof.—A similar experiment has been reported in this issue by Farolfi *et al.*, [40].

*Corresponding author.
craman@gatech.edu
†These authors contributed equally to this work.

[1] S. Burger, K. Bongs, S. Dettmer, W. Ertmer, K. Sengstock, A. Sanpera, G. V. Shlyapnikov, and M. Lewenstein, Phys. Rev. Lett. **83**, 5198 (1999).
[2] J. Denschlag, Science **287**, 97 (2000).
[3] Z. Dutton, Science **293**, 663 (2001).
[4] B. P. Anderson, P. C. Haljan, C. A. Regal, D. L. Feder, L. A. Collins, C. W. Clark, and E. A. Cornell, Phys. Rev. Lett. **86**, 2926 (2001).
[5] K. E. Strecker, G. B. Partridge, A. G. Truscott, and R. G. Hulet, Nature (London) **417**, 150 (2002).
[6] L. Khaykovich, Science **296**, 1290 (2002).
[7] S. L. Cornish, S. T. Thompson, and C. E. Wieman, Phys. Rev. Lett. **96**, 170401 (2006).
[8] S. Marcovitch and B. Reznik, Phys. Rev. A **78**, 052303 (2008).
[9] H. Landa, A. Retzker, T. Schaetz, and B. Reznik, Phys. Rev. Lett. **113**, 053001 (2014).
[10] C. S. Gardner, J. M. Greene, M. D. Kruskal, and R. M. Miura, Phys. Rev. Lett. **19**, 1095 (1967).
[11] T. Dauxois and M. Peyrard, *Physics of Solitons* (Cambridge University Press, Cambridge, UK, 2006).
[12] S. Ansoldi and E. I. Guendelman, Found. Phys. **37**, 712 (2007).
[13] B. Deng, V. Tournat, P. Wang, and K. Bertoldi, Phys. Rev. Lett. **122**, 044101 (2019).
[14] S. Trillo, E. M. Wright, G. I. Stegeman, and S. Wabnitz, Opt. Lett. **13**, 871 (1988).
[15] D. Christodoulides, Phys. Lett. **132A**, 451 (1988).
[16] M. H. Jakubowski, K. Steiglitz, and R. Squier, Computing with classical soliton collisions, in *Advances in Unconventional Computing. Emergence, Complexity and Computation*, edited by A. Adamatzky (Springer International Publishing, Cham, Switzerland, 2017), Vol. 23, pp. 297–307, https://doi.org/10.1007/978-3-319-33921-4_12.
[17] T. Busch and J. R. Anglin, Phys. Rev. Lett. **87**, 010401 (2001).
[18] C. Becker, S. Stellmer, P. Soltan-Panahi, S. Dörscher, M. Baumert, E.-M. Richter, J. Kronjäger, K. Bongs, and K. Sengstock, Nat. Phys. **4**, 496 (2008).
[19] A. Weller, J. P. Ronzheimer, C. Gross, J. Esteve, M. K. Oberthaler, D. J. Frantzeskakis, G. Theocharis, and P. G. Kevrekidis, Phys. Rev. Lett. **101**, 130401 (2008).
[20] D. J. Frantzeskakis, J. Phys. A **43**, 213001 (2010).
[21] C. Hamner, J. J. Chang, P. Engels, and M. A. Hoefer, Phys. Rev. Lett. **106**, 065302 (2011).

[22] D. Yan, J. J. Chang, C. Hamner, M. Hoefer, P. G. Kevrekidis, P. Engels, V. Achilleos, D. J. Frantzeskakis, and J. Cuevas, J. Phys. B **45**, 115301 (2012).
[23] I. Danaila, M. A. Khamehchi, V. Gokhroo, P. Engels, and P. G. Kevrekidis, Phys. Rev. A **94**, 053617 (2016).
[24] D. M. Stamper-Kurn and M. Ueda, Rev. Mod. Phys. **85**, 1191 (2013).
[25] A. M. Kamchatnov, Y. V. Kartashov, P.-É. Larré, and N. Pavloff, Phys. Rev. A **89**, 033618 (2014).
[26] C. Qu, L. P. Pitaevskii, and S. Stringari, Phys. Rev. Lett. **116**, 160402 (2016).
[27] K. Fujimoto, R. Hamazaki, and M. Ueda, Phys. Rev. Lett. **122**, 173001 (2019).
[28] T. M. Bersano, V. Gokhroo, M. A. Khamehchi, J. D'Ambroise, D. J. Frantzeskakis, P. Engels, and P. G. Kevrekidis, Phys. Rev. Lett. **120**, 063202 (2018).
[29] B. Xiong and J. Gong, Phys. Rev. A **81**, 033618 (2010).
[30] See Supplemental Material at http://link.aps.org/supplemental/10.1103/PhysRevLett.125.030402 for more details, which includes Refs. [31–34].
[31] A. Vinit, E. M. Bookjans, C. A. R. Sá de Melo, and C. Raman, Phys. Rev. Lett. **110**, 165301 (2013).
[32] A. Vinit and C. Raman, Phys. Rev. A **95**, 011603(R) (2017).
[33] E. M. Bookjans, A. Vinit, and C. Raman, Phys. Rev. Lett. **107**, 195306 (2011).
[34] D. A. Steck, available online http//steck.us/alkalidata (revision 2.1.5, 2015).
[35] S. Knoop, T. Schuster, R. Scelle, A. Trautmann, J. Appmeier, M. K. Oberthaler, E. Tiesinga, and E. Tiemann, Phys. Rev. A **83**, 042704 (2011).
[36] B. Arora, M. S. Safronova, and C. W. Clark, Phys. Rev. A **76**, 052509 (2007).
[37] G. E. Marti, A. MacRae, R. Olf, S. Lourette, F. Fang, and D. M. Stamper-Kurn, Phys. Rev. Lett. **113**, 155302 (2014).
[38] J. H. Kim, D. Hong, and Y.-i. Shin, arXiv:1907.10289.
[39] S. Stellmer, C. Becker, P. Soltan-Panahi, E.-M. Richter, S. Dörscher, M. Baumert, J. Kronjäger, K. Bongs, and K. Sengstock, Phys. Rev. Lett. **101**, 120406 (2008).
[40] A. Farolfi, D. Trypogeorgos, C. Mordini, G. Lamporesi, and G. Ferrari, preceding Letter, Phys. Rev. Lett. **125**, 030401 (2020).